Shaping Quantum Pulses of Light Via Coherent Atomic Memory

M. D. Eisaman,[1] L. Childress,[1] A. André,[1] F. Massou,[1] A. S. Zibrov,[1,2,3] and M. D. Lukin[1]

[1]*Physics Department, Harvard University, Cambridge, Massachusetts 02138, USA*
[2]*Harvard-Smithsonian Center for Astrophysics, Cambridge, Massachusetts 02138, USA*
[3]*P. N. Lebedev Institute of Physics, Moscow, 117924, Russia*

(Received 13 June 2004; published 30 November 2004)

We describe proof-of-principle experiments demonstrating a novel approach for generating pulses of light with controllable photon numbers, propagation direction, timing, and pulse shapes. The approach is based on preparation of an atomic ensemble in a state with a desired number of atomic spin excitations, which is later converted into a photon pulse. Spatiotemporal control over the pulses is obtained by exploiting long-lived coherent memory for photon states and Electromagnetically Induced Transparency in an optically dense atomic medium. Using photon counting experiments, we observe Electromagnetically Induced Transparency based generation and shaping of few-photon sub-Poissonian light pulses.

DOI: 10.1103/PhysRevLett.93.233602 PACS numbers: 42.50.Gy, 03.67.–a, 42.50.Dv

In recent years much effort has been directed toward generating quantum-mechanical states of the electromagnetic field with a well-defined number of quanta (i.e., photon number or Fock states). Motivated in part by the ideas of quantum information science, tremendous progress has been made in generating single-photon states by using photon pairs in parametric down-converters [1], single emitters [2,3], and single atoms in high-finesse cavities [4,5]. While parametric down-conversion techniques have recently been used to generate multiphoton states [6], it remains experimentally challenging to implement schemes that allow for simultaneous control over both photon number and spatiotemporal properties of the pulse.

In this Letter we describe proof-of-principle experiments demonstrating a novel approach for generating pulses of light with controllable, well-defined photon numbers, propagation direction, timing, and pulse shapes. These experiments exploit long-lived coherent memory for photon states in an optically dense atomic medium [7] and combine different aspects of earlier studies on "light storage" [8,9] and Raman preparation and retrieval of atomic excitations [10–15]. Our experiments expand previous studies on Electromagnetically Induced Transparency (EIT) based control of light propagation [8,9,16,17] into the domain of few-photon nonclassical light pulses.

In our approach we first optically pump a large ensemble of N atoms with a three-state "lambda" configuration of atomic states [see Fig. 1(a)] in the ground state $|g\rangle$. Spontaneous Raman scattering [18] is induced by a weak, off-resonant laser beam with Rabi frequency Ω_W and detuning Δ_W, referred to as the write laser. This two-photon process flips an atomic spin into the metastable state $|s\rangle$ while producing a correlated frequency-shifted photon (a so-called Stokes photon). Energy and momentum conservation ensure that for each Stokes photon emitted in certain direction there exists exactly one flipped spin quantum in a well-defined spin-wave mode. The number of spin-wave quanta and the number of photons in the Stokes field thus exhibit strong correlations, analogous to the correlations between photons emitted in parametric down-conversion [19]. As a result, measurement of the Stokes photon number n_S ideally projects the spin wave into a nonclassical collective state with n_S spin quanta [10]. After a controllable delay time τ_d [see Fig. 1(b)], the stored spin wave can be coherently converted into a light pulse by applying a second near-

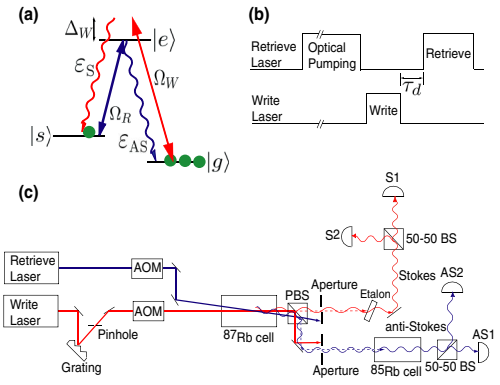

FIG. 1 (color online). Experimental procedure and apparatus. (a) ^{87}Rb levels used in the experiments (D_1 line): $|g\rangle = |5^2S_{1/2}, F = 1\rangle$, $|s\rangle = |5^2S_{1/2}, F = 2\rangle$, and $|e\rangle$ corresponds to $|5^2P_{1/2}, F' = 1\rangle$ and $|5^2P_{1/2}, F' = 2\rangle$. The write (retrieve) laser and Stokes (anti-Stokes) beam are labeled Ω_W (Ω_R) and ε_S (ε_{AS}), respectively. The write (retrieve) laser has a waist of 100 μm (1 mm). $\Delta_W \approx 1$GHz. (b) After the optical pumping pulse (provided by the retrieve laser), the 1.6μs-long write pulse is followed by the retrieve pulse after a controllable delay τ_d. (c) Schematic of the experimental setup. The write and retrieve lasers overlap at a small angle (~ 10 mrad) inside a magnetically-shielded ^{87}Rb vapor cell held at $\approx 75\,^\circ$C. AOM is acousto-optical modulator. PBS is polarizing beam splitter. S1, S2 (AS1, AS2) are avalanche photodetectors (APDs) for the Stokes (anti-Stokes) channel.

resonant laser beam with Rabi fequency Ω_R (retrieve laser), see Fig. 1(a). The physical mechanism for this retrieval process involves EIT [16,20–23] and is identical to that employed in previous experiments [8,9]. The direction, delay time τ_d, and rate of retrieval are determined by the direction, timing, and intensity of the retrieve laser, allowing control over the spatiotemporal properties of the retrieved pulse (referred to as the anti-Stokes pulse). Since the storage and retrieval processes ideally result in identical photon numbers in the Stokes and anti-Stokes pulses [21], this technique should allow preparation of an n-photon Fock state in the anti-Stokes pulse conditioned on detection of n Stokes photons.

The experimental apparatus [see Fig. 1(c)] is similar to that used in our earlier work [11]. The primary experimental challenge lies in transmitting the few-photon Stokes and anti-Stokes pulses while simultaneously blocking the write and retrieve laser beams. A polarizing beam splitter separates the write (retrieve) laser from the Stokes (anti-Stokes) Raman light, and further filtering is provided by an etalon or an optically-pumped ^{87}Rb cell in the write channel, and a ^{85}Rb cell in the read channel; this combined filtering separates the write (retrieve) laser from the Stokes (anti-Stokes) Raman light to one part in 10^9 (10^{12}). Experimentally, we take advantage of the long coherence time of the atomic memory (~ 3 μs in the present experiment, see Fig. 3) to create few-photon pulses with long coherence lengths ($\sim$few μs) that significantly exceed the time-resolution of the APDs ($\sim$50 ns). This allows us to directly count the photon-number in each of the pulses and to directly measure the pulse shapes by averaging the time-resolved avalanche photodetector (APD) output over many experimental runs.

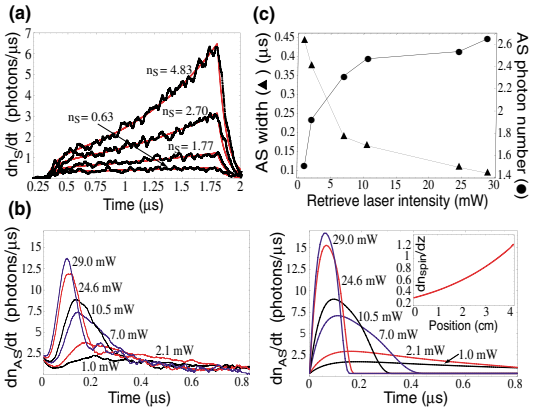

FIG. 2 (color online). Stokes and anti-Stokes pulse shapes. (a) Experimentally measured and theoretically calculated values of the Stokes photon flux dn_S/dt. For each plot, $n_S = \int dt\, dn_S/dt$ represents the total number of photons emitted from the cell. Write laser power was varied from 25 μW to 100 μW. (b) Experimentally measured (left) and theoretically calculated (right) values of the anti-Stokes photon flux dn_{AS}/dt. The experimental pulse shapes correspond to a Stokes pulse with $n_S \approx 3$ photons, and the theoretical curves assume an initial spin-wave with $n_{spin} = 3$ excitations and an optical depth of $\simeq 20$. Each curve is labeled with the power of the retrieve laser. (b and inset) Theoretical calculation of the number of flipped spins per unit length dn_{spin}/dz (cm^{-1}) for $n_{spin} = 3$. (c) Measured anti-Stokes pulse width (full-width at half-max) and total photon number as a function the retrieve laser intensity.

Figure 2(a) shows the average number of detected Stokes photons per unit time (photon flux) in the write channel as a function of time during the 1.6 μs-long write pulse. The magnitude of the photon flux is controlled by varying the excitation intensity. The shape of the Stokes pulse changes qualitatively as the total number of photons in the pulse exceeds unity: for pulses containing on average one photon or less, the flux is constant in time, whereas, for pulses containing more than one photon, the flux increases with time.

The observed evolution of the Stokes pulses can be understood qualitatively by considering the mutual growth of the photon field and spin excitation: the first flipped spin *stimulates* subsequent spin excitations which are accompanied by increased probability of Stokes photon emission. This process is governed by the collective Raman scattering rate $\xi = \eta|\Omega_W|^2\gamma/\Delta_W^2$, which is equal to the product of the optical depth η and the single atom scattering rate $|\Omega_W|^2\gamma/\Delta_W^2$, where γ is the decay rate of $|e\rangle$. For short excitation times t, we consider the evolution of several Hermite-Gaussian modes of Stokes radiation [18], and find that the photon flux is given by $dn_s/dt = \bar{N}\xi(1 + \xi t + \ldots)$, where $\bar{N}$ is the effective number of transverse modes (from experimental measurements we infer $\bar{N} \sim 4$). This prediction for dn_s/dt agrees with our observation that the flux will increase with time for $n_s \sim \xi t \geq 1$. The transition from a spontaneous to stimulated nature of the Stokes process also affects the spatial distribution of the atomic spin wave. For $n_s \leq 1$ the excitation is calculated to be uniformly distributed in the cell,

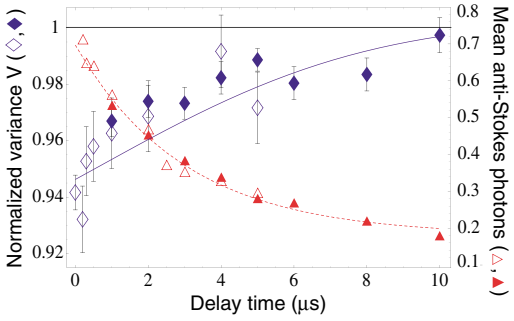

FIG. 3 (color online). Observation of nonclassical correlations. Normalized variance V (diamonds) and mean number of anti-Stokes photons (triangles) versus delay time τ_d. The open and filled symbols represent two experimental runs with similar experimental parameters. The dashed line is an exponential fit (characteristic time ~ 3 μs) to the mean number of anti-Stokes photons. The solid line is the result of a theoretical model described in the text.

while for $n_s > 1$ the spin-wave amplitude grows toward the end of the cell [see inset to Fig. 2(b)]. The observed dynamics provide evidence for the collective nature of the atomic spin excitations.

After a time delay τ_d, we apply the retrieve beam to convert the stored spin wave into anti-Stokes photons. Figure 2(b) demonstrates that the duration and peak flux of the anti-Stokes pulse can be controlled via the intensity of the retrieve laser. The resonant retrieve laser converts the spin coherence into a dark-state polariton, and eventually into an anti-Stokes photon. Note that the retrieve laser establishes an EIT configuration for the generated anti-Stokes field, so that the anti-Stokes light propagates unabsorbed through the cell. In the ideal limit of perfect EIT and large optical depth, the temporal shape of the anti-Stokes pulse is equivalent to the spatial shape of the atomic spin coherence, delayed by the time required to propagate out of the atomic cell at the group velocity $v_g(t) \propto |\Omega_R(t)|^2$ [23]. For larger (smaller) retrieve laser intensity, the excitation is released faster (slower), while the amplitude changes in such a way that the total number of anti-Stokes photons is always equal to the number of spin-wave excitations. In practice, decay of the spin coherence during the delay time τ_d and finite optical depth flatten and broaden the anti-Stokes pulse, reducing the total number of anti-Stokes photons which can be retrieved within the coherence time of the atomic memory, as indicated by theoretical calculations [Fig. 2(b)] based on Ref. [23]. The detailed comparison between theory and experiment in Fig. 2 suggests that the bandwidth of the generated anti-Stokes pulse is close to being Fourier-transform limited, while the transverse profile effectively corresponds to only a few spatial modes.

At fixed laser intensities and durations, the number of Stokes and anti-Stokes photons fluctuates from event to event in a highly correlated manner [11]. In order to quantify these correlations, we directly compare the number of Stokes and anti-Stokes photons for a large number of pulsed events (each with identical delay times τ_d and laser parameters). The variance of the resulting distributions is then compared to the photon shot noise level $\mathrm{PSN}_{th} = \bar{n}_S + \bar{n}_{AS}$, which represents the maximum degree of correlations possible for classical states [24]. We experimentally determine the photon shot noise for each channel by using a 50-50 beam splitter and two APDs per detection channel [see Fig. 1(c)] which allows us to accurately determine the measured $\mathrm{PSN}_{meas} = \mathrm{var}(AS1 - AS2) + \mathrm{var}(S1 - S2)$ value for each experiment. To quantify the correlations, we consider the normalized variance $V = \mathrm{var}[(n_{AS} - n_S)]/\mathrm{PSN}_{meas}$, which is one for classically correlated pulses and zero for pulses exhibiting perfect number correlations. Using this method, we measure $V = 0.942 \pm 0.006$ for the data shown in Fig. 3 at delay time $\tau_d = 0$ [25].

Figure 3 shows the normalized variance V as a function of storage time τ_d. Nonclassical correlations ($V < 1$) between Stokes and anti-Stokes pulses are clearly observed for storage times up to a few microseconds. The time scale over which the correlations decay is determined by the coherence properties of the atomic spin wave; nonclassical correlations are obtained only as long as the coherence of the stored excitation is preserved. Figure 3 also shows that the retrieval efficiency (the ratio of the average number of anti-Stokes photons to the average number of Stokes photons) decreases in a similar manner as τ_d is increased. A fit to this time dependence (dashed line) yields a characteristic decoherence time $1/\gamma_c$ of about 3 μs, consistent with the time scale for atomic diffusion from the write laser beam. These results demonstrate that within the spin coherence time, it is possible to control the timing between preparation and retrieval, while preserving nonclassical correlations.

It is important to note that at $\tau_d = 0$ the observed value $V = 0.942 \pm 0.006$ is far from the ideal value of $V = 0$. One source of error is the finite retrieval efficiency, which is limited by two factors. Because of the atomic memory decoherence rate γ_c, the finite retrieval time τ_r always results in a finite loss probability $p \approx \gamma_c \tau_r$. Moreover, even as $\gamma_c \to 0$ the retrieval efficiency is limited by the finite optical depth η of the ensemble, which yields an error scaling as $p \sim 1/\sqrt{\eta}$. The anti-Stokes pulses in Fig. 3 have widths on the order of the measured decoherence time, so the atomic excitation decays before it is fully retrieved. The measured maximum retrieval efficiency at $\tau_d = 0$ corresponds to about 0.3.

In addition to finite retrieval efficiency, other factors reduce correlations, including losses in the detection system, background photons, APD afterpulsing effects, and imperfect mode matching. To understand the effects of such imperfections, we consider a theoretical model which incorporates loss, background, and several spatial modes. Based on experimental measurements, the overall detection efficiency α and number of background photons n_{BG} used in the model are $\alpha_S = 0.07$, $n_S^{BG} = 0.3$ ($\alpha_{AS} = 0.21$, $n_{AS}^{BG} = 0.12$) on the Stokes (anti-Stokes) channel, with a retrieval efficiency decay time of 3 μs and four transverse spatial modes assumed. The results of this model are represented by the solid line in Fig. 3, and agree quite well with experimental observation.

Losses arise from decoherence of the atomic memory, imperfect transmission through the filtering etalon (Stokes) and ^{85}Rb cell (anti-Stokes), and coupling into the detection fibers. Background is caused by imperfect filtering of the write and retrieve lasers, as well as a four-wave mixing process resulting from the undesired coupling of the $|g\rangle$ and $|e\rangle$ states by the retrieve laser. Improved filtering (via higher-Q etalons, for example) has the potential to reduce both loss and background.

The correlations between Stokes and anti-Stokes pulses allow for the conditional preparation of the anti-Stokes pulse with intensity fluctuations that are suppressed compared with classical light. In order to quantify the per-

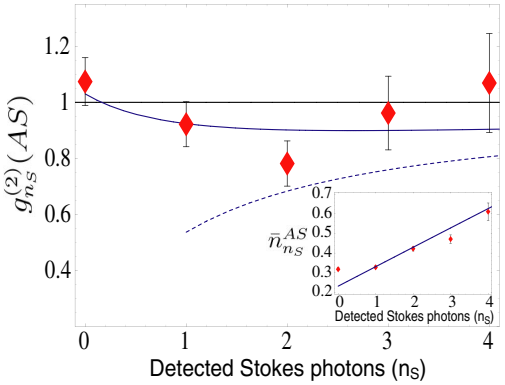

FIG. 4 (color online). Conditional nonclassical state generation. Diamonds show experimentally measured values $g^{(2)}(AS) = \langle AS_1 \cdot AS_2\rangle / \langle AS_1\rangle\langle AS_2\rangle$ [see Fig. 1(c)] as a function of the number of detected Stokes photons. The measured mean photons numbers were $\bar{n}_S = 1.06$ and $\bar{n}_{AS} = 0.36$. The solid line shows the result of a theoretical model [26]. (Inset) Measured mean anti-Stokes number $\bar{n}^{AS}_{n_S}$ conditioned on the Stokes photon-number n_S. The solid line represents $\bar{n}^{AS}_{n_S}$ as predicted by the model.

formance of this technique, we measured the second-order intensity correlation function $g^{(2)}_{n_S}(AS)$ and mean number of photons $\bar{n}^{AS}_{n_S}$ for the anti-Stokes pulse conditioned on the detection of n_S photons in the Stokes channel (see Fig. 4). (For classical states of light, $g^{(2)} \geq 1$, whereas, an ideal Fock state with n photons has $g^{(2)} = 1 - 1/n$.) Note that the mean number of anti-Stokes photons grows linearly with n_S, while $g^{(2)}_{n_S}(AS)$ drops below unity, indicating the nonclassical character of the anti-Stokes photon states. In the presence of background counts, $g^{(2)}_{n_S}(AS)$ does not increase monotonically with n_S, but instead exhibits a minimum at $n_S = 2$. The Mandel Q parameter [24] can be calculated using $Q^{AS}_{n_S} = \bar{n}^{AS}_{n_S}[g^{(2)}_{n_S}(AS) - 1]$; from the measurements we determine $Q^{AS}_{n_S=2} = -0.09 \pm 0.03$ for conditionally generated states with $n_S = 2$ ($Q \geq 0$ for classical states and $Q = -1$ for Fock states). Experimental imperfections such as loss and background can be accounted for in a theoretical model [26] that yields reasonable agreement with experimental observations (solid curve in Fig. 4). Using this model corrected for loss and background on the retrieval channel (dashed line in Fig. 4), we estimate $(\bar{n}^{AS}_{n_S=2}, Q^{AS}_{n_S=2})$ to be approximately $(2.5, -0.85)$.

Although the corrected parameters are closer to the ideal limit, they still do not correspond to a perfect Fock state. This is due to loss and background in the preparation channel, which prevent measurement of the exact number of created spin excitations. In principle, the conditional state preparation can be made insensitive to overall Stokes detection efficiency α_S by working in the regime of a very weak excitation [10]; however, Stokes channel background counts n^{BG}_S prevent one from reaching this regime in practice. A qualitative condition for high quality Fock state generation, $\zeta \equiv n^{BG}_S(1 - \alpha_S)/n_S\alpha_S \ll 1$, is only marginally fulfilled in our experiments ($\zeta \sim 0.3$), accounting for the imperfectly prepared atomic states. Refinements in the Stokes detection system and better transverse mode selection should permit conditional Fock state generation with significantly improved purity, potentially providing a basic building block for long-distance quantum communication [10].

We gratefully acknowledge T. Zibrova, J. MacArthur, D. Phillips, R. Walsworth, P. Hemmer, A. Trifonov, and C. van der Wal for useful discussions and experimental help. This work was supported by the DARPA, the NSF, the MIT-Harvard CUA, the Packard, Sloan, and Hertz Foundations, and École des Mines de Paris (FM).

[1] C. K. Hong and L. Mandel, Phys. Rev. Lett. **56**, 58 (1986).
[2] P. Michler *et al.*, Science **290**, 2282 (2000).
[3] C. Santori *et al.*, Nature (London) **419**, 594 (2002).
[4] A. Kuhn, M. Hennrich, and G. Rempe, Phys. Rev. Lett. **89**, 067901 (2002).
[5] J. McKeever *et al.*, Science **303**, 1992 (2004).
[6] E. Waks *et al.*, Phys. Rev. Lett. **92**, 113602 (2004).
[7] M. D. Lukin, Rev. Mod. Phys. **75**, 457 (2003).
[8] C. Liu *et al.*, Nature (London) **409**, 490 (2001).
[9] D. F. Phillips *et al.*, Phys. Rev. Lett. **86**, 783 (2001).
[10] L. M. Duan *et al.*, Nature (London) **414**, 413 (2001).
[11] C. H. van der Wal *et al.*, Science **301**, 196 (2003).
[12] A. Kuzmich *et al.*, Nature (London) **423**, 731 (2003).
[13] C.W. Chou *et al.*, Phys. Rev. Lett. **92**, 213601 (2004).
[14] W. Jiang *et al.*, Phys. Rev. A **69**, 043819 (2004).
[15] S.V. Polyakov *et al.*, quant-ph/0406050.
[16] S. E. Harris, Phys. Today **50**, 736 (1997).
[17] D. A. Braje *et al.*, Phys. Rev. A **68**, 041801 (2003).
[18] M. G. Raymer and I. A. Walmsley, in *Progress in Optics*, edited by E. Wolf (North-Holland, Amsterdam, 1996), Vol. 28, p. 181.
[19] D. T. Smithey *et al.*, Phys. Rev. Lett. **69**, 2650 (1992).
[20] M. O. Scully and M. S. Zubairy, *Quantum Optics* (Cambridge University Press, Cambridge, England, 1997).
[21] M. D. Lukin *et al.*, Phys. Rev. Lett. **82**, 1847 (1999).
[22] K. J. Boller, A. Imamoglu, and S. E. Harris, Phys. Rev. Lett. **66**, 2593 (1991).
[23] M. Fleischhauer and M. D. Lukin, Phys. Rev. Lett. **84**, 5094 (2000).
[24] L. Mandel and E. Wolf, *Optical Coherence and Quantum Optics* (Cambridge University Press, Cambridge, England, 1995).
[25] For the experimental conditions of Fig. 3, we estimate that dead-time effects reduce the measured $\bar{n}_{AS}$ by 2.5% from its actual value and increase $V = \mathrm{var}[(n_{AS} - n_S)]/\mathrm{PSN}_{meas}$ by less than 0.2% from its actual value (well within the ~0.6% error bars).
[26] Parameters used in the model (estimated from experimental measurements): $\alpha_S = 0.35$, $n^{BG}_S = 0.27$ ($\alpha_{AS} = 0.1$, $n^{BG}_{AS} = 0.12$) on the Stokes (anti-Stokes) channel.